Title
π-Facial Selectivities in Hydride Reductions of Hindered Endocyclic Iminium Ions

Journal
The Journal of Organic Chemistry, 84(1)

ISSN
0022-3263

Authors
Chen, Shuming
Chan, Amy Y
Walker, Morgan M
et al.

Publication Date
2019-01-04

DOI
10.1021/acs.joc.8b02603

Peer reviewed

HHS Public Access

Author manuscript

J Org Chem. Author manuscript; available in PMC 2020 January 04.

Published in final edited form as:

J Org Chem. 2019 January 04; 84(1): 273–281. doi:10.1021/acs.joc.8b02603.

π-Facial Selectivities in Hydride Reductions of Hindered Endocyclic Iminium Ions

Shuming Chen[†], **Amy Y. Chan**[‡], **Morgan M. Walker**[‡], **Jonathan A. Ellman**[*,‡], and **K. N. Houk**[*,†]

[†]Department of Chemistry and Biochemistry, University of California, Los Angeles, California 90095-1569, United States

[‡]Department of Chemistry, Yale University, New Haven, Connecticut 06520, United States

Abstract

The origins of π-facial selectivities in the borohydride reduction of endocyclic iminium ions have been elucidated by density functional theory calculations. In reductions of conjugated ("thermodynamic") iminium ions, the π-facial preference of the hydride attack was found to be due to torsional steering. Attack at the favored π-face leads to a lower-energy "half-chair"-like conformation of the tetrahydropyridine product, whereas attack at the other π-face results in an unfavorable "twist-boat" conformation. In reductions of nonconjugated ("kinetic") iminium ions, torsional distinction is small between the top- and bottom-face attacks, and the π-facial selectivity of the hydride approach is primarily due to steric hindrance.

Graphical Abstract

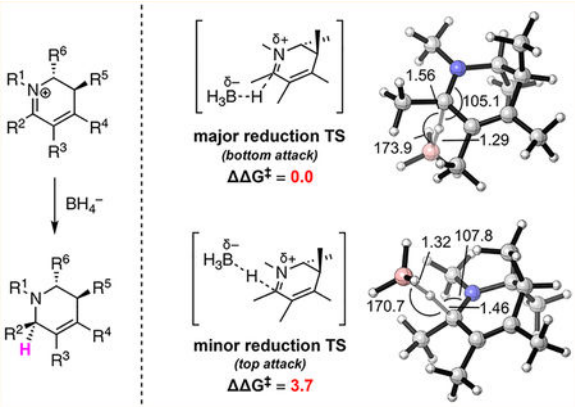

[*]**Corresponding Authors:** jonathan.ellman@yala.edu (J.A.E.)., houk@chem.ucla.edu (K.N.H.).

Supporting Information

The Supporting Information is available free of charge on the ACS Publications website at DOI: 10.1021/acs.joc.8b02603.

Computational details, energies, Cartesian coordinates of computed structures, and NMR spectra (PDF)

The authors declare no competing financial interest.

INTRODUCTION

Nonaromatic nitrogen heterocycles, such as piperidines, are prevalent motifs in pharmaceuticals that have a wide impact on human health.[1–4] Much of modern synthetic chemistry research seeks to improve the ability to access such pharmaceutically privileged molecular scaffolds with high levels of stereocontrol.[5] To this end, one of our groups disclosed diastereoselective entries into highly substituted tetrahydropyridines via the reduction of endocyclic iminium ions (Scheme 1).[6,7] Starting from α,β-unsaturated imine and alkyne inputs (1 and 2), a Rh(I)-catalyzed C–H alkenylation/6π-aza-electro-cyclization sequence furnished 1,2-dihydropyridines 3. By tuning the acidity of the proton source as well as varying equilibration times, these dihydropyridines can be protonated regio- and stereoselectively at either C3 or C5, affording "kinetic" and "thermodynamic" iminium ions. The nonconjugated "kinetic" iminium ion is formed under more strongly acidic conditions and shorter equilibration times. Alternatively, *in situ* reduction of the kinetically formed iminium can be accomplished without equilibration by using $NaBH(OAc)_3$ and AcOH. The conjugated "thermodynamic" iminium ion is obtained under more weakly acidic conditions and/or with longer equilibration times. The structures and relative stereochemistry of these iminium ions have been confirmed by X-ray crystallographic analysis and density functional theory (DFT) computations.[7] Both the "kinetic" and the "thermodynamic" iminium ions undergo reduction by hydride sources with high π-facial selectivities to yield tetrahydropyridines with high *dr* (in most cases >95:5). The excellent *dr* values observed cannot always be rationalized based on steric arguments. We therefore undertook a combined computational and experimental study to elucidate the origins of π-facial selectivities in the reduction of these iminium ions.

COMPUTATIONAL METHODS

Computations were performed with Gaussian 09.[8] Molecular geometries were optimized using the M06–2X[9] functional and the 6–31+G(d,p) basis set. The effect of solvation on molecular geometries was accounted for during optimizations using the SMD[10] solvation model with either ethanol or tetrahydrofuran as the solvent. Frequency analyses were carried out at the same level of theory as that used for geometry optimizations to characterize the stationary points as either minima (no imaginary frequencies) or saddle points (one imaginary frequency) on the potential energy surface, and to obtain ZPE, thermal corrections, and entropies to obtain the Gibbs free energies. Intrinsic Reaction Coordinate (IRC) calculations were performed to ensure that the saddle points located were transition states connecting the reactants and the products. Single point energies were calculated with the M06–2X functional and the def2-TZVPP[11] basis set, and solvation effects were modeled using the SMD solvation model. Molecular structures were visualized using CYLview.[12] Reiterative Monte Carlo conformational searches were performed with the Merck molecular force field (MMFF) implemented in Spartan '16, followed by DFT reoptimizations, to ensure that the lowest energy conformations of intermediates and transition states were obtained. Calculations performed with the ωB97XD[13] and B3LYP[14]-D3[15] functionals, as well as a more detailed discussion on alternative conformers explored in this study, are provided in the Supporting Information.

RESULTS AND DISCUSSION

Reduction of "Thermodynamic" Iminium Ions.

The "thermodynamic" iminium ions **4** are characterized by a conjugated N=C−C=C unit and *trans* alkyl substituents at C5 and C6. The calculated lowest-energy structures of both **4a** and **4b** show that these iminium ions adopt a "twist-boat" conformation with both the C5 and C6 substituents pseudo-axial (Figure 1). The geometries of these "thermodynamic" iminium ions do not offer immediate clues as to why the bottom-face hydride attack is favored; if anything, a bottom-face approach appears to be less desirable given that the C6 alkyl group is closer to the C2 hydride addition site than the C5 alkyl group is.

Figure 2 shows the calculated transition states for the borohydride reduction of iminium **4b**, which serves as a simplified computational model of **4a**. In both transition states, the borohydride nucleophile approaches the iminium along the anticipated Bürgi–Dunitz trajectory (105–108° angles). The C5 and C6 methyl groups occupy pseudo-axial positions in both TSs due to $A^{1,2}$-strain. Hydride attack from the bottom face (**TS-1-major**) is predicted to be favored by 3.7 kcal/mol, which is in good agreement with the experimentally observed >95:5 *dr* ($\Delta\Delta G^{\ddagger}$ > 2.2 kcal/mol).[5] This energy difference is difficult to rationalize based on steric hindrance alone. We instead turned our attention to torsional effects, which are known to govern stereoselectivities in additions to endocyclic unsaturated electrophiles.[16]

To probe the conformational preferences of the six-membered base ring throughout the borohydride reduction event, we examined the analogous reaction in the unsubstituted parent system. The Intrinsic Reaction Coordinate (IRC) of the borohydride reduction of the unsubstituted parent iminium is shown in Figure 3. This iminium ion adopts a "twist-boat"-like conformation with an N1–C2–C3–C4 dihedral angle of 14.3°. This nonplanarity of the π-system appears to be a compromise to allow the molecule to maintain a staggered conformation about the C5–C6 bond. As the reaction progresses, the N1–C2–C3–C4 dihedral decreases and becomes negative, and the ring structure gradually transitions to a "half-chair" tetrahydropyridine. The "half-chair" conformation is known to be preferred by cyclohexene and analogous rings over the "twist-boat" by 5–6 kcal/mol.[17]

An examination of the conformations adopted by the sixmembered base rings show that, in **TS-1-major**, the ring conformation is more "half-chair"-like, whereas, in **TS-1-minor**, it instead resembles a "twist-boat" (Figure 2). Snapshots of substrate geometries along the IRCs of these TSs confirm that they indeed evolve toward very different tetrahydropyridine conformations (Figure 4). The bottom-face attack results in a decrease in the N1–C2–C3–C4 dihedral angle paralleling that observed in the unsubstituted system (Figure 3). As a result of this change, the ring structure transitions to a "half-chair"-like conformation in the post-reaction complex. In contrast, the top-face attack follows a trajectory that *increases* the N1–C2–C3–C4 angle. Rather than arriving at the low-energy "half-chair", the ring structure becomes "twist-boat"-like in the post-reaction complex. Two unfavorable near-eclipsing interactions exist in the "twist-boat"-like tetrahydropyridine in the post-reaction complex, rendering it high in energy (Figure 4). These results show that an important reason for the favorability of **TS-1-major** is that it connects to a more "half-chair"-like, and therefore

lower-energy, tetrahydropyridine conformation. This is roughly analogous to *trans*-diaxial attack on a half-chair cyclohexene, which evolves to a “chair” cyclohexane rather than a “boat” cyclohexane.

But what is preventing the base ring from transitioning toward the “half-chair” in the top-face attack scenario? As shown in Figure 4 and Scheme 2, nucleophilic addition from the top face results in C2 pyramidalizing “upwards”, and the forming C–N single bond dipping downward. This motion leads to a “twist-boat” tetrahydropyridine conformation. Conversely, bottom-face attack results in C2 pyramidalizing “downwards”, which is the motion required to evolve toward a “half-chair” tetrahydropyridine. In order for the upward C2 pyramidalization to connect to a “half-chair” conformation, the iminium ion must first flip to the alternative “twist-boat” where both C5 and C6 are pseudo-equatorial, and incur an energetic cost as high as 5.4 kcal/mol due to $A^{1,2}$-strain interactions.

We calculated reduction TSs of two modified iminium ions, **4c** and **4d** (Scheme 3), where one of the two $A^{1,2}$-strain interactions has been removed. In both cases, bottom-face attack is still favored, but diastereodistinction is diminished to 1.8 kcal/mol, 1.9 kcal/mol weaker than in the system with two $A^{1,2}$-strain interactions (Figure 5). This result shows that the number of $A^{1,2}$-strain interactions determines the degree of diastereofacial distinction through torsional control.

If the number of $A^{1,2}$-strain interactions is indeed what controls torsional, and therefore π-facial, selectivity in nucleophilic additions to these endocyclic iminium ions, structural modifications that do not impact the number of $A^{1,2}$-strain interactions should have little effect on diastereodistinction. We tested this hypothesis both computationally and experimentally with two modified systems. Iminium **4e**, which is unsubstituted at the C3 position, still possesses two $A^{1,2}$-strain interactions (Scheme 3). Calculated TSs for the borohydride reduction of **4e** indicate that bottom-face attack is preferred by 3.2 kcal/mol (Figure 6a), which is very close to the 3.7 kcal/mol difference observed for the reduction of **4b**. Snapshots along the IRCs show that the same torsional effects control the evolution of substrate geometries, with the bottom-face attack being favored because it leads to the lower-energy “half-chair”-like conformation of the product. A comparably substituted iminium ion is found experimentally to undergo preferential bottom-face hydride addition with >95:5 *dr* (Figure 6b), confirming the computational predictions.

We also calculated TSs for the borohydride reduction of iminium **4f**, where the C6 substituent is changed to a bulky *tert*-butyl group (Figure 7a). Even though a more hindered C6 substituent would be expected to disfavor nucleophile approach from the bottom face, the bottom-face attack is still calculated to be favored by 3.3 kcal/mol. An examination of substrate geometry snapshots along the IRCs reveals that the *tert*-butyl group does not change the nature of the torsional distinction between the two TSs. Experimentally, a comparably substituted iminium ion with a C6 *tert*-butyl group is found to undergo borohydride reduction preferentially at the bottom face with >95:5 *dr* (Figure 7b). This result confirms that the diastereofacial selectivity in this system is insensitive to steric modifications that do not fundamentally alter the $A^{1,2}$-strain interactions.

Reduction of “Kinetic” Iminium Ions.

Borohydride reductions of the “kinetic” iminium ions present a very different torsional landscape (Scheme 4). The unconjugated “kinetic” iminium ions are locked in their “boat” conformations by up to four $A^{1,2}$-strain interactions between the alkyl substituents (Scheme 3). Top- and bottom-face nucleophilic attack would both lead to “half-chair”-like conformations of the product. Because these two “half-chairs” are close in energy, torsional distinction between the top- and bottom-face attack TSs is expected to be small, and steric hindrance should instead control the diastereofacial selectivity.

Consistent with this prediction, our calculated TSs for the borohydride reduction of iminium ion **5a** show that the attack from the less hindered top face is preferred by 1.3 kcal/mol (Figure 8). This value is in excellent agreement with the experimentally observed 90:10 *dr* ($\Delta\Delta G^{\ddagger}$ = 1.3 kcal/mol). Snapshots of substrate geometries along the IRCs confirm that torsional distinction between the TSs is small, as both top- and bottom-face attack lead to “half-chair”-like tetrahydropyridine conformations.

CONCLUSIONS

We have elucidated the origins of π-facial selectivities in hydride reductions of endocyclic iminium ions through DFT calculations. Reductions of conjugated (“thermodynamic”) iminium ions were found to be diastereoselective due to torsional steering. Hydride attack from the bottom face (Figure 2) is favored because it leads to a lower-energy “half-chair”-like conformation of the tetrahydropyridine product, which lowers the TS energy. In contrast, top-face attack results in an unfavorable “twist-boat” conformation, leading to a higher-energy TS. We show that the number of $A^{1,2}$-strain interactions present in the ring determines the magnitude of the bottom-face preference, and modifications that do not significantly impact these $A^{1,2}$-strain interactions have little effect on diastereoselectivity. Despite the dense substitution in these ring systems, steric hindrance only determines π-facial selectivity in cases where torsional distinction between top and bottom-face attacks is small, such as in the case of the nonconjugated (“kinetic”) iminium ions.

EXPERIMENTAL SECTION

General Methods.

For air-sensitive experiments, all glassware was dried at 150 °C for at least 12 h and allowed to cool under an inert atmosphere. Experiments were set up inside a glovebox under a nitrogen atmosphere with oxygen and moisture levels not exceeding 2 ppm. Solvents for air-sensitive reactions were dried by passing through activated alumina, degassed, and stored over 3 Å molecular sieves in a glovebox. Solvents of ACS reagent grade were used for workup and purification. Alkynes and liquid amines were distilled under a nitrogen atmosphere or *in vacuo*, and stored in a glovebox prior to use. $[RhCl(coe)_2]_2$ was purchased from Strem and stored inside a N_2-filled inert atmosphere glovebox at −25 °C. The ligand, *p*-$Me_2N–C_6H_4–PEt_2$, was purchased from Sigma-Aldrich and stored inside a N_2-filled inert atmosphere glovebox at −25 °C. Stock solutions of the rhodium catalyst were prepared by dissolving $[RhCl(coe)_2]_2$ (200 mg, 279 μmol) and *p*-$Me_2N–C_6H_4–PEt_2$ (117 mg, 558 μmol)

in anhydrous toluene until a total volume of 6.0 mL was reached. Stock solutions could be used immediately after mixing, and showed no difference in catalytic activity after being stored for months in a −25 °C freezer inside a N_2-filled glovebox. NMR characterization was performed on 400 or 500 MHz instruments. Data are reported in the following format: chemical shift in ppm, multiplicity (s = singlet, d = doublet, t = triplet, q = quartet, m = multiplet, dd = doublet of doublets, etc.), coupling constant *J* in hertz, and integration. All spectra were referenced against residual solvent peaks (^{1}H: residual $CDCl_3$ = 7.26 ppm).

N-(1,2-Dimethyl-2-buten-1-ylidene)-benzenemethanamine (1a).

The following protocol is based on a literature procedure.[18] A 100 mL round-bottom flask equipped with a magnetic stir bar was charged with (*E*)-3-methylpent-3-en-2-one (1.089 g, 11.10 mmol, 1.00 equiv), anhydrous THF (9.0 mL), and titanium(IV) ethoxide (12 mL, 57 mmol, 5.2 equiv). Inside a N_2-filled glovebox, a 4 mL vial was charged with benzylamine (1.249 g, 11.65 mmol, 1.05 equiv), capped, and taken to the fume hood. The vial was opened to air, and the contents were transferred to the round-bottom flask. The flask was sealed with a septum and heated to 55 °C for 2 h and then allowed to cool to rt. *N*,*N*,*N*′,*N*′-Tetrakis(2-hydroxyethyl)ethylenediamine (EDTE) (13.5 mL, 62.8 mmol, 5.66 equiv) was added, and the mixture was heated to 55 °C for 15 min until a clear yellow solution was observed. The mixture was cooled to rt and poured into a separatory funnel containing NH_4OH (60 mL) and brine (30 mL). The aqueous phase was extracted with EtOAc (90 mL), and the organic layer was washed with brine (2 × 60 mL), dried over Mg_2SO_4, filtered, and concentrated *in vacuo*. The residue was filtered through basic Al_2O_3 (eluting with pentane), and the filtrates were concentrated *in vacuo* to give **1a** as a yellow oil (1.052 g, 5.617 mmol, 51%), which was stored at −25 °C under a N_2 atmosphere in a glovebox. ^{1}H NMR (400 MHz, $CDCl_3$): δ 7.39−7.35 (m, 2H), 7.35−7.29 (m, 2H), 7.25−7.19 (m, 1H), 6.18 (q, *J* = 6.9 Hz, 1H), 4.63 (s, 2H), 2.04 (s, 3H), 1.94 (s, 3H), 1.81 (d, *J* = 6.9 Hz, 3H). The spectroscopic data agree with previously reported literature data.[18]

N-(1-Methyl-3-phenyl-2-propen-1-ylidene)-benzenemethanamine (1b).

The following protocol is based on a literature procedure.[6] A 20 mL scintillation vial wrapped in aluminum foil and equipped with a magnetic stir bar was charged with 4-phenyl-3-buten-2-one (541 mg, 3.70 mmol, 1.00 equiv), anhydrous THF (2.8 mL), and titanium(IV) ethoxide (4.0 mL, 19 mmol, 5.1 equiv). Inside a N_2-filled glovebox, a 4 mL vial was charged with benzylamine (417 mg, 3.89 mmol, 1.05 equiv), capped, and taken to the fume hood. The vial was opened to air, and the contents were transferred to the scintillation vial. The vial was rinsed with anhydrous THF (2 × ca. 0.1 mL), and the washings were likewise transferred to the scintillation vial. The vial was sealed with a septum and heated to 55 °C for 2 h and then allowed to cool to rt. EDTE (4.5 mL, 22 mmol, 5.9 equiv) was added, and the mixture was heated to 55 °C for 15 min until a clear yellow solution was observed. The mixture was cooled to rt and poured into a separatory funnel containing NH_4OH (20 mL) and brine (10 mL). The aqueous phase was extracted with EtOAc (30 mL), and the organic layer was washed with brine (2 × 20 mL), dried over Mg_2SO_4, filtered, and concentrated *in vacuo*. The residue was filtered through basic Al_2O_3 (eluting with pentane), and the filtrates were concentrated *in vacuo* to give **1b** as a yellow oil (441 mg, 1.87 mmol, 51%), which was stored in an 8 mL vial wrapped in aluminum foil at

−25 °C under a N_2 atmosphere in a glovebox. ^{1}HNMR (400 MHz, $CDCl_3$): δ 7.56−7.50 (m, 2H), 7.44−7.21 (m, 8H), 7.09 (d, J = 16.6 Hz, 1H), 7.00 (d, J = 17.1 Hz, 1H), 4.69 (s, 2H), 2.19 (s, 3H). The spectroscopic data agree with previously reported literature data.[6]

(2*R*,3*S*,6*R*)-1-Benzyl-2,3-diethyl-4,5,6-trimethyl-1,2,3,6-tetrahydropyridine (6b-exp).

Inside a N_2-filled glovebox, a 4 mL vial was charged with *N*-(1,2-dimethyl-2-buten-1-ylidene)-benzene-methanamine (46.8 mg, 250 μmol, 1.00 equiv), and the contents were transferred to a J. Young NMR tube equipped with a benzene-d_6 capillary (for locking and shimming). The vial was rinsed with toluene (3 × ca. 0.1 mL), and the washings were likewise transferred to the J. Young tube. Rh stock solution (see General Methods) (67 μL, 6.3 μmol, 2.5 mol %) followed by 3-hexyne (34 μL, 300 μmol, 1.2 equiv) were added to the J. Young tube. Toluene was added until the total volume reached ca. 0.6 mL. The J. Young tube was quickly capped, and the contents were thoroughly mixed. The J. Young tube was then taken to a fume hood where it was heated at 100 °C for 2 h, at which point analysis by ^{1}H NMR indicated complete conversion to the 1,2-dihydropyridine. In a glovebox, a flame-dried 20 mL scintillation vial equipped with a magnetic stir bar was charged with $(PhO)_2PO_2H$ (131 mg, 525 μmol, 2.10 equiv) and anhydrous THF (1.0 mL). The dihydropyridine reaction mixture was then added. The J. Young tube was rinsed with anhydrous THF (2 × ca. 0.2 mL), and the washings were likewise transferred to the vial. The vial was sealed with a septum, and the reaction mixture was stirred for 16 h at rt to ensure complete conversion to the C5-protonated iminium ion. The vial was then taken to a fume hood and placed under a N_2 atmosphere. Separately, a flame-dried 20 mL scintillation vial equipped with a magnetic stir bar was charged with Bu_4NBH_4 (315 mg, 1.23 mmol, 4.90 equiv) on the benchtop, sealed with a septum, and then placed under a N_2 atmosphere. Anhydrous THF (3.1 mL) was added to the vial, and the mixture was cooled to 0 °C. To the well-stirred solution of Bu_4NBH_4, the contents of the iminium ion solution were transferred dropwise via a syringe and needle. The vial was rinsed with anhydrous THF (2 × ca. 0.2 mL), and the washings were likewise transferred to the well-stirred solution of Bu_4NBH_4. The reaction mixture was stirred at 0 °C for a further 2 h and then allowed to warm to room temperature over 2 h. The reaction was quenched with H_2O (H_2 evolution), and the resulting mixture was basified with 1 M aq. NaOH until a pH of ca. 11 was reached. The mixture was extracted with hexanes/EtOAc/Et_3N (400:25:3, 3 × 10 mL), and the combined organic layers were dried over $MgSO_4$, filtered, and concentrated *in vacuo*. A known quantity of 2,6-dimethoxytoluene was then added as an external standard. Crude ^{1}H NMR analysis provided **6b-exp** in 72% NMR yield (>95% dr). The spectroscopic data agree with previously reported literature data.[7]

(2*R*,3*S*,6*R*)-1-Benzyl-2,3-diethyl-6-methyl-4-phenyl-1,2,3,6-tetrahydropyridine (6e-exp).

Inside a N_2-filled glovebox, a 4 mL vial was charged with *N*-(1-methyl-3-phenyl-2-propen-1-ylidene)-benzenemethanamine (79.4 mg, 337 μmol, 1.00 equiv), and the contents were transferred to a J. Young NMR tube equipped with a benzene-d_6 capillary (for locking and shimming). The vial was rinsed with toluene (3 × ca. 0.1 mL), and the washings were likewise transferred to the J. Young tube. Rh stock solution (see General Methods) (134 μL, 12.5 μmol, 5.00 mol %) followed by 3-hexyne (46 μL, 404 μmol, 1.2 equiv) were added to the J. Young tube. Toluene was added until the total volume reached ca. 0.6 mL. The J.

Young tube was quickly capped, and the contents were thoroughly mixed. The J. Young tube was then taken to a fume hood where it was heated at 100 °C for 2 h, at which point analysis by ^{1}H NMR indicated complete conversion to the 1,2-dihydropyridine. In a glovebox, a 4 mL vial was charged with $(PhO)_2PO_2H$ (151 mg, 605 μmol, 1.80 equiv) and anhydrous THF (1.2 mL). The contents of the vial were thoroughly mixed and then transferred to the J. Young tube containing the dihydropyridine reaction mixture. The vial was rinsed with anhydrous THF (2 × ca. 0.1 mL), and the washings were likewise transferred to the J. Young tube. The J. Young tube was capped, and the contents were thoroughly mixed. The J. Young tube was then taken to a fume hood where it was heated at 50 °C for 1 h, at which point analysis by ^{1}H NMR indicated complete conversion to the C5-protonated iminium ion. Separately, a flame-dried 20 mL scintillation vial equipped with a magnetic stir bar was charged with Bu_4NBH_4 (244 mg, 0.948 mmol, 2.81 equiv) on the benchtop, sealed with a septum, and then placed under a N_2 atmosphere. Anhydrous THF (1.4 mL) was added to the vial, and the mixture was cooled to 0 °C. To the well-stirred solution of Bu_4NBH_4, the contents of the iminium ion solution were transferred dropwise via a syringe and needle. The J. Young tube was rinsed with anhydrous THF (2 × ca. 0.2 mL), and the washings were likewise transferred to the well-stirred solution of Bu_4NBH_4. The reaction mixture was stirred at 0 °C for a further 2 h and then allowed to warm to room temperature over 2 h. The reaction was quenched with H_2O (H_2 evolution), and the resulting mixture was basified with 1 M aq. NaOH until a pH of ca. 11 was reached. The mixture was extracted with hexanes/EtOAc/Et_3N (200:25:3, 3 × 10 mL), and the combined organic layers were dried over $MgSO_4$, filtered, and concentrated *in vacuo*. The residue was filtered through a short plug of silica (ca. 5 cm in a Pasteur pipet, eluting with hexanes/EtOAc/Et_3N (200:25:3)), and the filtrate was concentrated *in vacuo*. A known quantity of 2,6-dimethoxytoluene was then added as an external standard. Crude ^{1}H NMR analysis provided **6e-exp** in 74% NMR yield (>95% dr). The spectroscopic data agree with previously reported literature data.[19]

(2*S*,3*S*,6*R*)-1-Benzyl-2-(tert-butyl)-3,4,5,6-tetramethyl-1,2,3,6-tetrahydropyridine (6f-exp).

Inside a N_2-filled glovebox, a 4 mL vial was charged with *N*-(1,2-dimethyl-2-buten-1-ylidene)-benzenemethanamine (46.8 mg, 250 μmol, 1.00 equiv), and the contents were transferred to a J. Young NMR tube equipped with a benzene-d_6 capillary (for locking and shimming). The vial was rinsed with toluene (3 × ca. 0.1 mL), and the washings were likewise transferred to the J. Young tube. Rh stock solution (see General Methods) (134 μL, 12.5 μmol, 5.00 mol %) followed by 4,4-dimethyl-2-pentyne (50 μL, 375 μmol, 1.5 equiv) were added to the J. Young tube. Toluene was added until the total volume reached ca. 0.6 mL. The J. Young tube was quickly capped, and the contents were thoroughly mixed. The J. Young tube was then taken to a fume hood where it was heated at 100 °C for 2 h, at which point analysis by ^{1}H NMR indicated complete conversion to the 1,2-dihydropyridine. In a glovebox, a flame-dried 20 mL scintillation vial equipped with a magnetic stir bar was charged with $(PhO)_2PO_2H$ (138 mg, 550 μmol, 2.20 equiv) and anhydrous THF (1.4 mL). The dihydropyridine reaction mixture was then added. The J. Young tube was rinsed with anhydrous THF (2 × ca. 0.2 mL), and the washings were likewise transferred to the vial. The vial was sealed with a septum, and the reaction mixture was stirred for 16 h at rt to ensure complete conversion to the C5-protonated iminium ion. The vial was then taken to a fume hood, and placed under a N_2 atmosphere. Separately, a flame-dried 20 mL scintillation vial

equipped with a magnetic stir bar was charged with Bu_4NBH_4 (315 mg, 1.23 mmol, 4.90 equiv) on the benchtop, sealed with a septum, and then placed under a N_2 atmosphere. Anhydrous THF (4.1 mL) was added to the vial, and the mixture was cooled to 0 °C. To the well-stirred solution of Bu_4NBH_4, the contents of the iminium ion solution were transferred dropwise via a syringe and needle. The vial was rinsed with anhydrous THF (2 × ca. 0.2 mL), and the washings were likewise transferred to the well-stirred solution of Bu_4NBH_4. The reaction mixture was stirred at 0 °C for a further 2 h and then allowed to warm to room temperature over 2 h. The reaction was quenched with H_2O (H_2 evolution), and the resulting mixture was basified with 1 M aq. NaOH until a pH of ca. 11 was reached. The mixture was extracted with hexanes/EtOAc/Et_3N (400:25:3, 3 × 10 mL), and the combined organic layers were dried over $MgSO_4$, filtered, and concentrated *in vacuo*. The residue was filtered through a short plug of silica (ca. 5 cm in a Pasteur pipet, eluting with hexanes/EtOAc/Et_3N (400:25:3)), and the filtrate was concentrated *in vacuo*. A known quantity of 2,6-dimethoxytoluene was then added as an external standard. Crude ^{1}H NMR analysis provided **6f-exp** in 69% NMR yield (>95% dr). The spectroscopic data agree with previously reported literature data.[7]

(2*S*,3*S*,6*R*)-1-Benzyl-5,6-diethyl-2,3,4-trimethyl-1,2,3,6-tetrahydropyridine (7a-exp).

Inside a N_2-filled glovebox, a 4 mL vial was charged with *N*-(1,2-dimethyl-2-buten-1-ylidene)-benzene-methanamine (93.6 mg, 500 μmol, 1.00 equiv), and the contents were transferred to a J. Young NMR tube equipped with a benzene-d_6 capillary (for locking and shimming). The vial was rinsed with toluene (3 × ca. 0.1 mL), and the washings were likewise transferred to the J. Young tube. Rh stock solution (see General Methods) (134 μL, 12.5 μmol, 5.00 mol %) followed by 3-hexyne (68.0 μL, 600 μmol, 1.2 equiv) were added to the J. Young tube. Toluene was added until the total volume reached ca. 0.6 mL, and the J. Young tube was quickly capped and the contents were thoroughly mixed. The J. Young tube was then taken to a fume hood where it was heated at 100 °C for 2 h, at which point analysis by ^{1}H NMR indicated complete conversion to the 1,2-dihydropyridine. In a fume hood, the contents of the J. Young tube were transferred to a flame-dried 50 mL round-bottom flask equipped with a magnetic stir bar. The J. Young tube was washed with EtOH (2 × 0.7 mL), and the washings were likewise transferred to the flask, which was sealed with a septum and placed under a N_2 atmosphere. Inside a N_2-filled glovebox, a 4 mL vial was charged with $PhSO_3H$ (238 mg, 1.50 mol, 3.00 equiv), sealed with a septum, and taken to the fume hood. The vial was placed under a N_2 atmosphere, EtOH (3.0 mL) was added, and the solution was transferred to the dihydropyridine reaction mixture via a syringe and needle. The reaction mixture was allowed to stir at rt for 15 min to ensure complete conversion to the C3-protonated iminium ion. The reaction mixture was then cooled to −78 °C. Separately, a flame-dried 20 mL scintillation vial was charged with Bu_4NBH_4 (514 mg, 2.00 mmol, 4.00 equiv) on the benchtop, sealed with a septum, and then placed under a N_2 atmosphere. EtOH (2.6 mL) was added to the vial, and the contents were transferred dropwise to the iminium ion solution. The vial was rinsed with EtOH (2 × ca. 0.2 mL), and the washings were likewise transferred to the iminium ion solution. The reaction mixture was stirred at −78 °C for 2 h, then allowed to warm to room temperature over 2 h. The reaction was quenched with H_2O (H_2 evolution), and the resulting mixture was basified with 1 M aq. NaOH until a pH of ca. 11 was reached. The mixture was extracted with EtOAc (3 × 20 mL), and the combined

organic layers were dried over $MgSO_4$, filtered, and concentrated *in vacuo*. A known quantity of 2,6-dimethoxytoluene was then added as an external standard. Crude ^1H NMR analysis provided **7a-exp** in 87% NMR yield (90% dr). The spectroscopic data of the major isomer agree with previously reported literature data.[6]

Supplementary Material

Refer to Web version on PubMed Central for supplementary material.

ACKNOWLEDGMENTS

K.N.H is grateful to the National Science Foundation (Grant CHE-1764328) for financial support. J.A.E. acknowledges support from from the NIH ((R35GM122473), and A.Y.C. is grateful for an ACS Division of Organic Chemistry Summer Undergraduate Research Fellowship. Calculations were performed on the Hoffman2 cluster at the University of California, Los Angeles, and the Extreme Science and Engineering Discovery Environment (XSEDE), which is supported by the National Science Foundation (Grant OCI-1053575).

REFERENCES

(1). Roughley SD; Jordan AM The Medicinal Chemist's Toolbox: An Analysis of Reactions Used in the Pursuit of Drug Candidates. J. Med. Chem 2011, 54, 3451. [PubMed: 21504168]

(2). Lovering F; Bikker J; Humblet C Escape from Flatland: Increasing Saturation as an Approach to Improving Clinical Success. J. Med. Chem 2009, 52, 6752. [PubMed: 19827778]

(3). Walters WP; Green J; Weiss JR; Murcko MA What Do Medicinal Chemists Actually Make? A 50-Year Retrospective. J. Med. Chem 2011, 54, 6405. [PubMed: 21755928]

(4). Ritchie TJ; Macdonald SJF The Impact of Aromatic Ring Count on Compound Developability – Are Too Many Aromatic Rings a Liability in Drug Design? Drug Discovery Today 2009, 14, 1011. [PubMed: 19729075]

(5). (a)For recent examples of stereoselective nitrogen heterocycle synthesis, see:Huang X; Li X; Xie X; Harms K; Riedel R; Meggers E Catalytic Asymmetric Synthesis of a Nitrogen Hetero-cycle Through Stereocontrolled Direct Photoreaction from Electronically Excited State. Nat. Commun 2017, 8, 2245. [PubMed: 29269853] (b)Feng J-J; Lin T-Y; Zhu C-Z; Wang H; Wu H-H; Zhang J The Divergent Synthesis of Nitrogen Heterocycles by Rhodium(I)-Catalyzed Intermolecular Cycloadditions of Vinyl Aziridines and Alkynes. J. Am. Chem. Soc 2016, 138, 2178. [PubMed: 26859710] (c)Munnuri S; Adebesin AM; Paudyal MP; Yousufuddin M; Dalipe A; Falck JR Catalyst-Controlled Diastereoselective Synthesis of Cyclic Amines via C–H Functionalization. J. Am. Chem. Soc 2017, 139, 18288. [PubMed: 29182870] (d)Tait MB; Butterworth S; Clayden J 2,2- and 2,6-Diarylpiperidines by Aryl Migration within Lithiated Urea Derivatives of Tetrahydropyridines. Org. Lett 2015, 17, 1236. [PubMed: 25692395] (e)Ballette R; Perez M; Proto S; Amat M; Bosch J Total Synthesis of (+)-Madangamine D. Angew. Chem., Int. Ed 2014, 53, 6202.(f)Duttwyler S; Chen S; Lu C; Mercado BQ; Bergman RG; Ellman JA Regio- and Stereoselective 1,2-Dihydropyridine Alkylation/Addition Sequence for the Synthesis of Piperidines with Quaternary Centers. Angew. Chem., Int. Ed 2014, 53, 3877.(g)Chen S; Bacauanu V; Knecht T; Mercado BQ; Bergman RG; Ellman JA New Regio- and Stereoselective Cascades via Unstabilized Azomethine Ylide Cycloadditions for the Synthesis of Highly Substituted Tropane and Indolizidine Frameworks. J. Am. Chem. Soc 2016, 138, 12664. [PubMed: 27642766]

(6). Duttwyler S; Lu C; Rheingold AL; Bergman RG; Ellman JA Highly Diastereoselective Synthesis of Tetrahydropyridines by a C–H Activation–Cyclization–Reduction Cascade. J. Am. Chem. Soc 2012, 134, 4064. [PubMed: 22356093]

(7). Duttwyler S; Chen S; Takase MK; Wiberg KB; Bergman RG; Ellman JA Proton Donor Acidity Controls Selectivity in Nonaromatic Nitrogen Heterocycle Synthesis. Science 2013, 339, 678. [PubMed: 23393259]

(8). Frisch MJ; Trucks GW; Schlegel HB; Scuseria GE; Robb MA; Cheeseman JR; Scalmani G; Barone V; Mennucci B; Petersson GA; Nakatsuji H; Caricato M; Li X; Hratchian HP; Izmaylov AF; Bloino J; Zheng G; Sonnenberg JL; Hada M; Ehara M; Toyota K; Fukuda R; Hasegawa J; Ishida M; Nakajima T; Honda Y; Kitao O; Nakai H; Vreven T; Montgomery JA Jr.; Peralta JE; Ogliaro F; Bearpark M; Heyd JJ; Brothers E; Kudin KN; Staroverov VN; Kobayashi R; Normand J; Raghavachari K; Rendell A; Burant JC; Iyengar SS; Tomasi J; Cossi M; Rega N; Millam JM; Klene M; Knox JE; Cross JB; Bakken V; Adamo C; Jaramillo J; Gomperts R; Stratmann RE; Yazyev O; Austin AJ; Cammi R; Pomelli C; Ochterski JW; Martin RL; Morokuma K; Zakrzewski VG; Voth GA; Salvador P; Dannenberg JJ; Dapprich S; Daniels AD; Farkas O, Foresman JB; Ortiz JV; Cioslowski J; Fox DJ Gaussian 09; Gaussian, Inc.: Wallingford, CT, 2009.

(9). Zhao Y; Truhlar DG The M06 Suite of Density Functionals for Main Group Thermochemistry, Thermochemical Kinetics, Noncovalent Interactions, Excited States, and Transition Elements: Two New Functionals and Systematic Testing of Four M06-Class Functionals and 12 Other Functionals. Theor. Chem. Acc 2008, 120, 215.

(10). Marenich AV; Cramer CJ; Truhlar DG Universal Solvation Model Based on Solute Electron Density and on a Continuum Model of the Solvent Defined by the Bulk Dielectric Constant and Atomic Surface Tensions. J. Phys. Chem. B 2009, 113, 6378. [PubMed: 19366259]

(11). Weigend F; Ahlrichs R Balanced Basis Sets of Split Valence, Triple Zeta Valence and Quadruple Zeta Valence Quality for H to Rn: Design and Assessment of Accuracy. Phys. Chem. Chem. Phys 2005, 7, 3297. [PubMed: 16240044]

(12). Legault CY CYLview, 1.0b; Universiteé de Sherbrooke: Sherbrooke, Quebec, Canada, 2009 http://www.cylview.org.

(13). Chai JD; Head-Gordon M Long-Range Corrected Hybrid Density Functionals with Damped Atom–Atom Dispersion Corrections. Phys. Chem. Chem. Phys 2008, 10, 6615. [PubMed: 18989472]

(14). (a)Head-Gordon M; Pople JA; Frisch MJ MP2 Energy Evaluation by Direct Methods. Chem. Phys. Lett 1988, 153, 503.(b)Becke AD Density-Functional Thermochemistry. III. The Role of Exact Exchange. J. Chem. Phys 1993, 98, 5648.(c)Lee C; Yang W; Parr RG Development of the Colle-Salvetti Correlation-Energy Formula into a Functional of the Electron Density. Phys. Rev. B: Condens. Matter Mater. Phys 1988, 37, 785.(d)Vosko SH; Wilk L; Nusair M Accurate Spin-Dependent Electron Liquid Correlation Energies for Local Spin Density Calculations: a Critical Analysis. Can. J. Phys 1980, 58, 1200.(e)Stephens PJ; Devlin FJ; Chabalowski CF; Frisch MJ Ab Initio Calculation of Vibrational Absorption and Circular Dichroism Spectra Using Density Functional Force Fields. J. Phys. Chem 1994, 98, 11623.

(15). Grimme S; Antony J; Ehrlich S; Krieg H A Consistent and Accurate ab initio Parametrization of Density Functional Dispersion Correction (DFT-D) for the 94 Elements H-Pu. J. Chem. Phys 2010, 132, 154104. [PubMed: 20423165]

(16). See: Wang H; Houk KN Torsional Control of Stereo-selectivities in Electrophilic Additions and Cycloadditions to Alkenes. Chem. Sci 2014, 5, 462and references cited within.

(17). Anet FAL; Freedberg DI; Storer JW; Houk KN On the Potential Energy Surface for Ring Inversion in Cyclohexene and Related Molecules. J. Am. Chem. Soc 1992, 114, 10969.

(18). Colby DA; Bergman RG; Ellman JA Synthesis of Dihydropyridines and Pyridines from Imines and Alkynes via C–H Activation. J. Am. Chem. Soc 2008, 130, 3645. [PubMed: 18302381]

(19). Chen S; Mercado BQ; Bergman RG; Ellman JA Regio-and Diastereoselective Synthesis of Highly Substituted, Oxygenated Piperidines from Tetrahydropyridines. J. Org. Chem 2015, 80, 6660. [PubMed: 26098485]

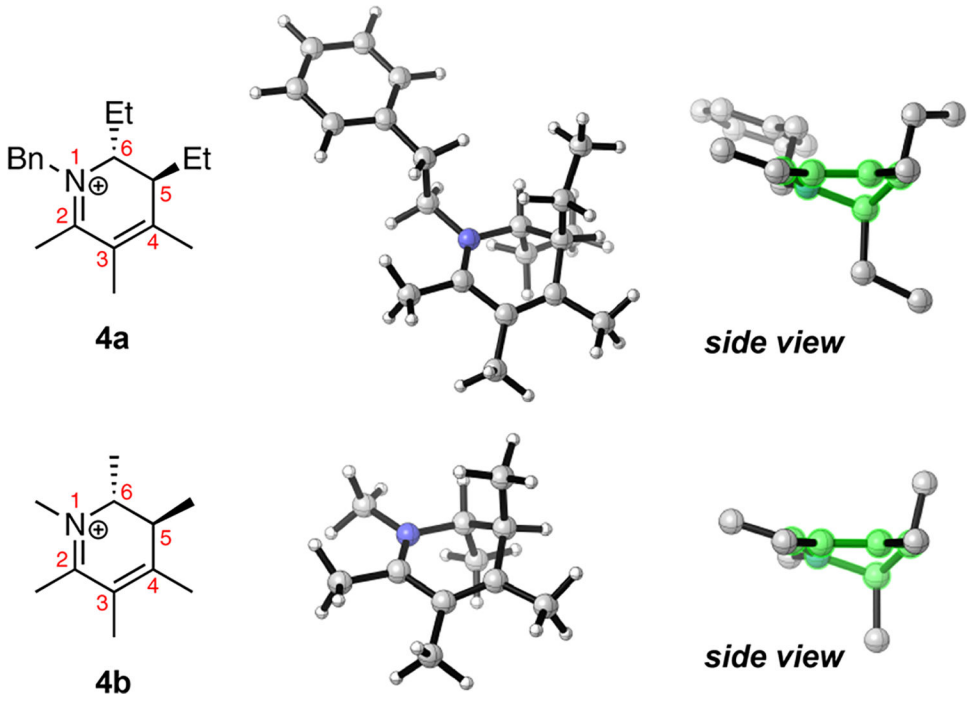

Figure 1.

Calculated global minimum structures of conjugated “thermodynamic” iminium ions. Side views are provided with all hydrogens attached to carbons omitted for clarity.

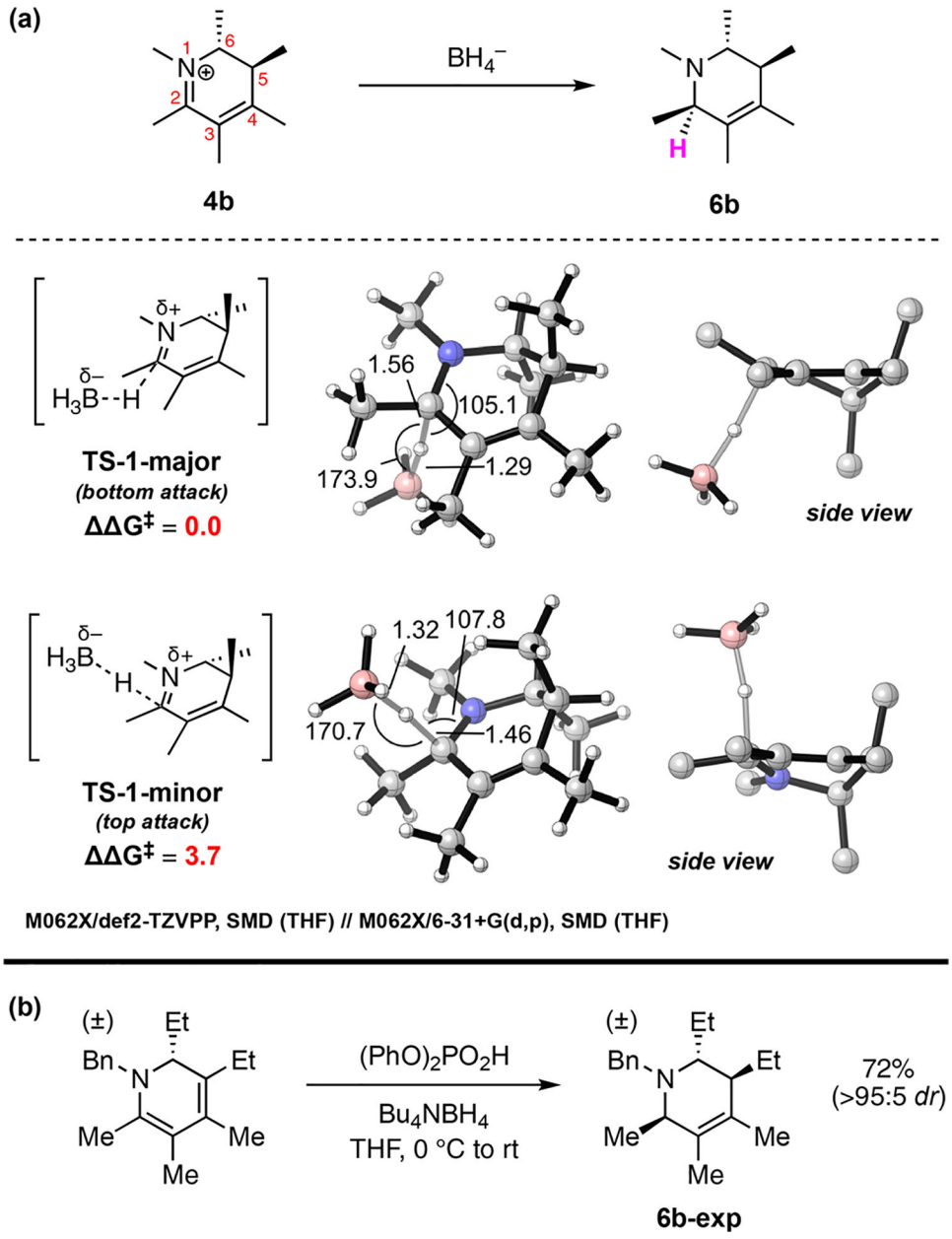

Figure 2.

(a) Calculated transition states for the reduction of a model "thermodynamic" iminium ion **4b** by BH_4^-. Side views are provided with all hydrogens attached to carbons omitted for clarity. Interatomic distances are denoted in ångströms, energies are given in kcal/mol, and angles are given in degrees. (b) Experimental *dr* from the borohydride reduction of a comparably substituted iminiumion.

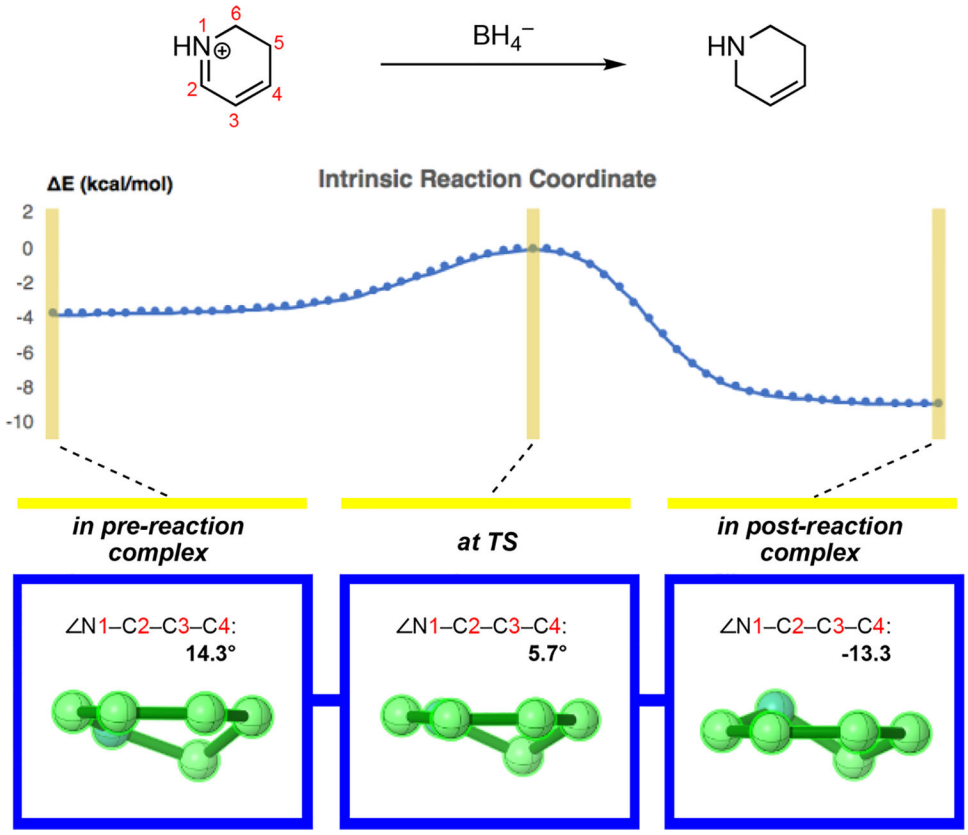

Figure 3.

Intrinsic Reaction Coordinate (IRC) of the borohydride reduction of an unsubstituted iminium ion, and snapshots of substrate geometry along the IRC. ΔE values are relative to TS-2 and obtained at the M06–2X/6–31+G(d,p) level of theory. Hydrogen atoms are omitted for clarity.

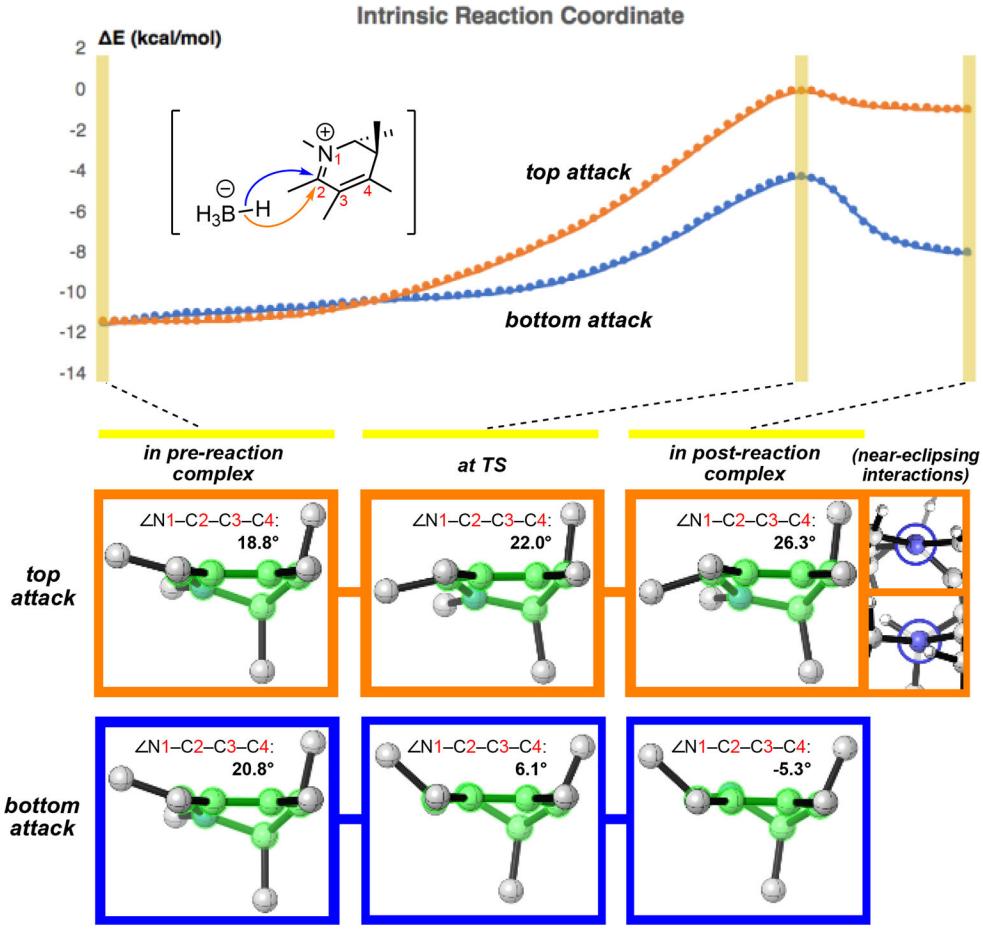

Figure 4.

Intrinsic Reaction Coordinates (IRCs) of reduction transition states **TS-1-major** (bottom-face attack) and **TS-1-minor** (top-face attack), and snapshots of substrate geometry along the IRCs. ΔE values are relative to **TS-1-minor** and obtained at the M06–2X/6–31+G(d,p) level of theory. Hydrogen atoms are omitted forclarity.

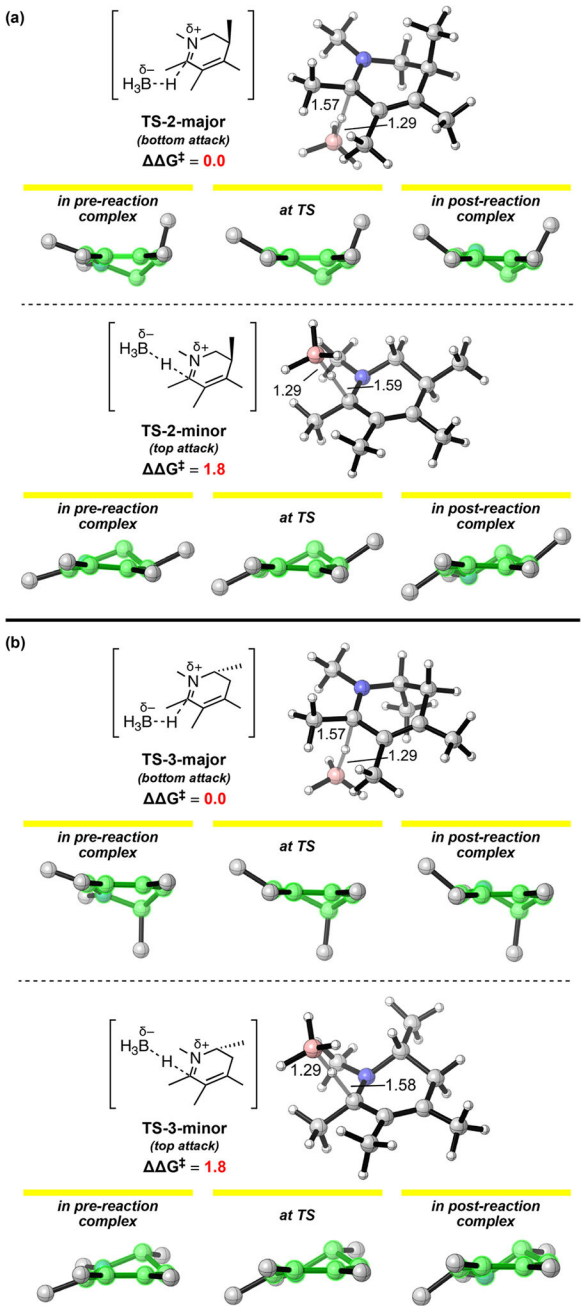

Figure 5.

Calculated transition states for the reductions of modified iminium ions **4c** and **4d** by BH_4^-, and IRC snapshots of substrate geometry (hydrogens are omitted for clarity). Interatomic distances are denoted in ångströms, and energies are given in kcal/mol.

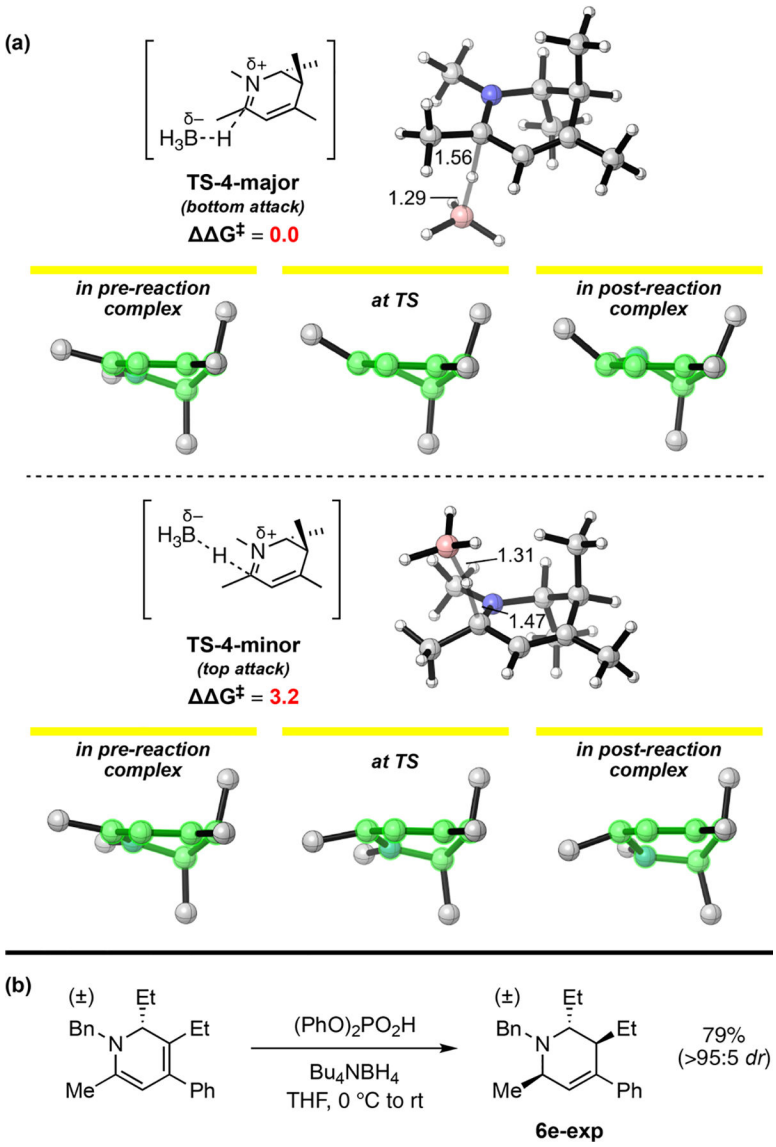

Figure 6.

(a) Calculated transition states for the reduction of iminium ion 4e by BH_4^-, and IRC snapshots of substrate geometry (hydrogens are omitted for clarity). Interatomic distances are denoted in ångströms, and energies are given in kcal/mol. (b) Experimental *dr* from the borohydride reduction of a comparably substituted iminiumion.

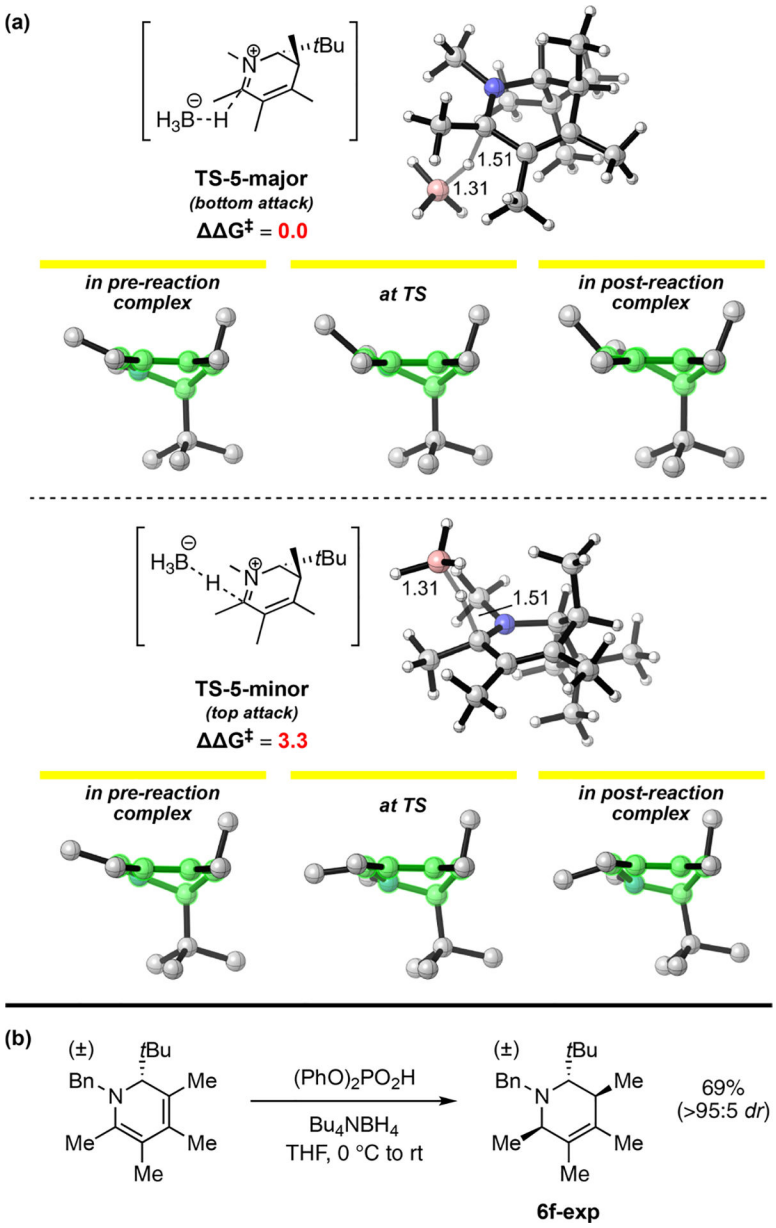

Figure 7.

(a) Calculated transition states for the reduction of iminium ion **4f** by BH_4^-, and IRC snapshots of substrate geometry (hydrogens are omitted for clarity). Interatomic distances are denoted in ångströms, and energies are given in kcal/mol. (b) Experimental *dr* from the borohydride reduction of a comparably substituted iminiumion.

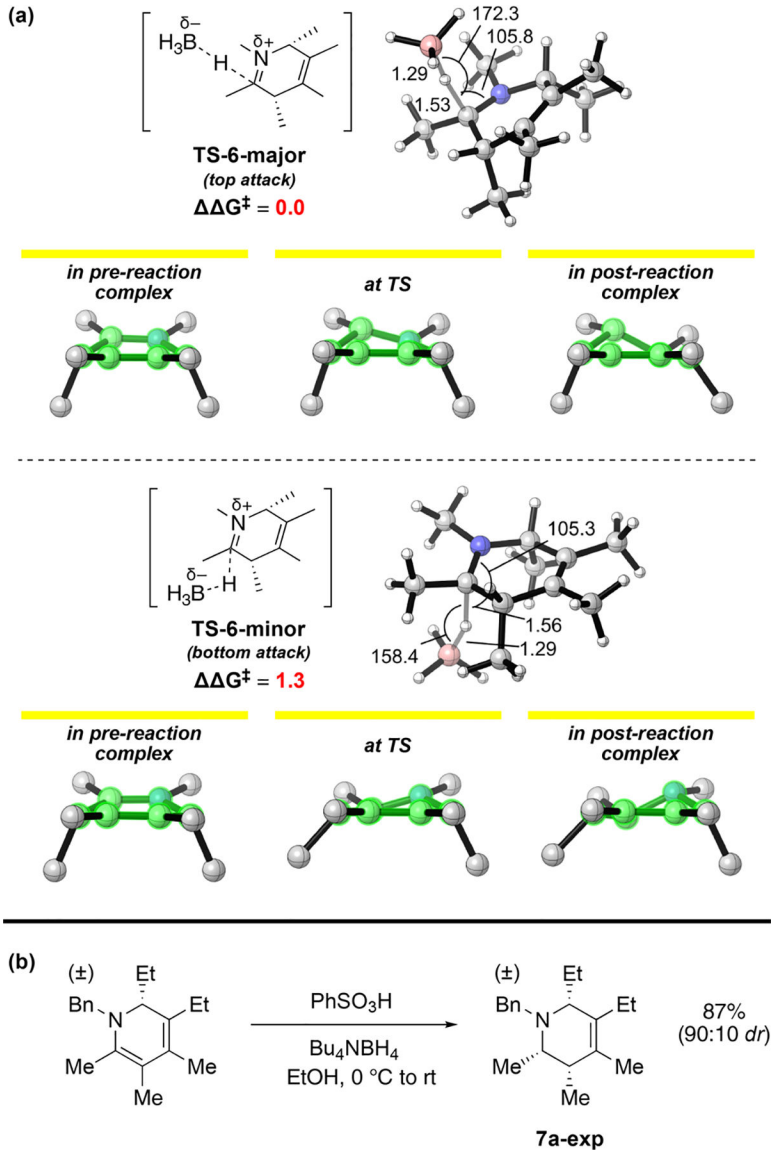

Figure 8.

(a) Calculated transition states for the reduction of iminium ion 5a by BH_4^-, and IRC snapshots of substrate geometry (hydrogens are omitted for clarity). Interatomic distances are denoted in ångströms, and energies are given in kcal/mol. (b) Experimental *dr* from the borohydride reduction of a comparably substituted iminiumion.

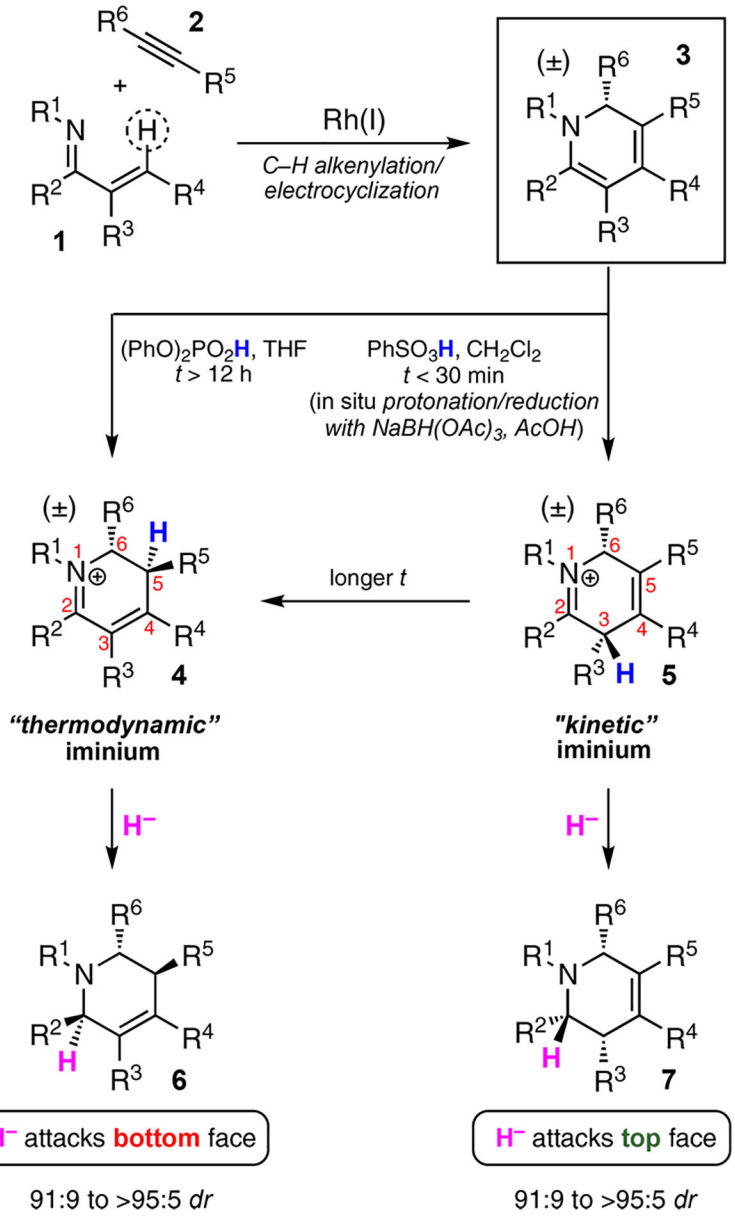

Scheme 1.

Regio- and Diastereodivergent Syntheses of Tetrahydropyridines

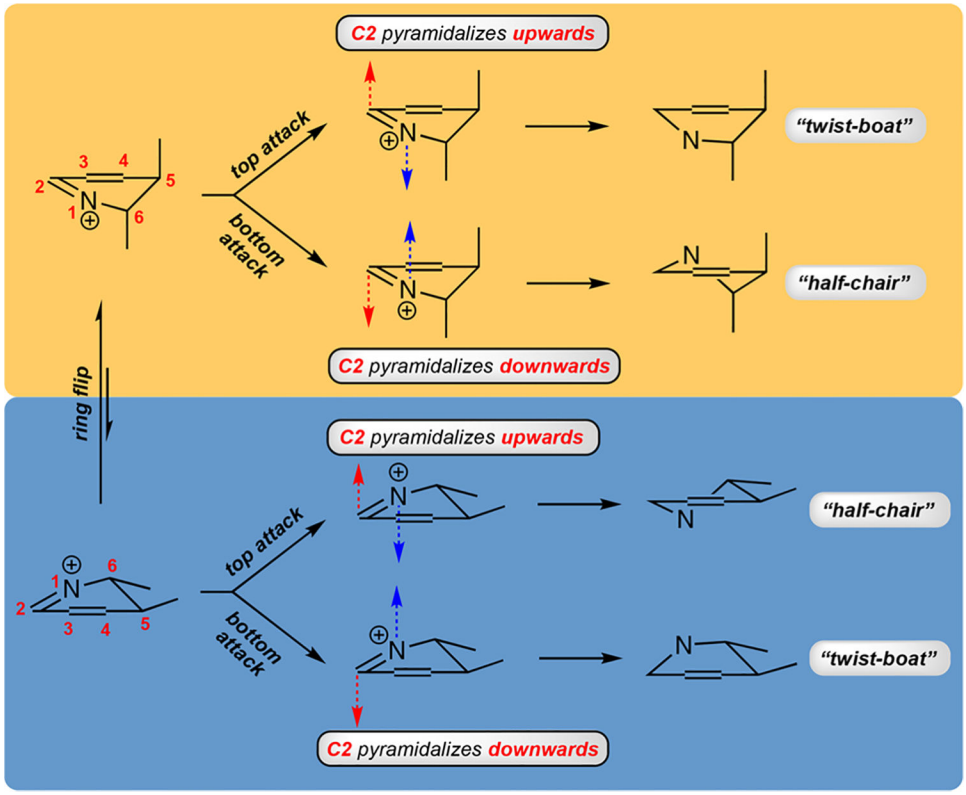

Scheme 2. Rationalization of Torsional Control in π-Facial Selective Hydride Additions to "Thermodynamic" Iminium Ions[a]

[a]Substituents are omitted for clarity except for C5 and C6 methyl groups.

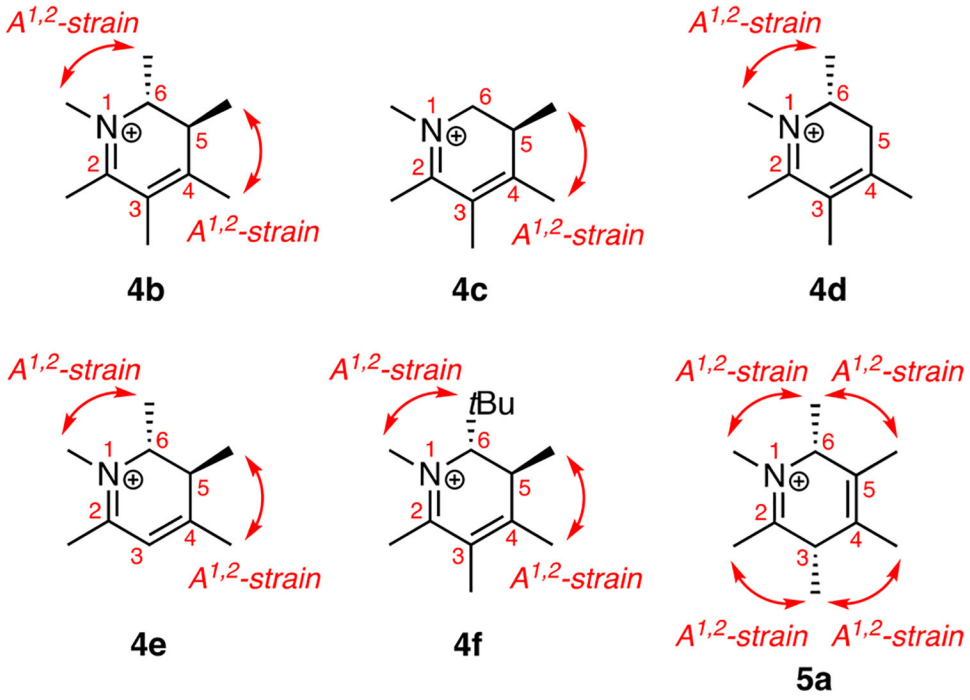

Scheme 3.
Hindered Iminium Ions Explored Computationally in This Study

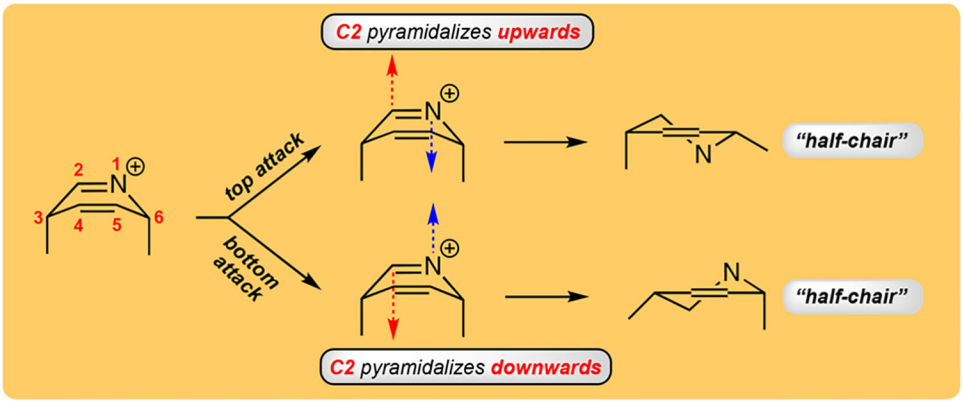

Scheme 4. Torsional Consequences of Top- and Bottom-Face Hydride Additions to "Kinetic" Iminium Ions[a]

[a]Substituents are omitted for clarity except for C3 and C6 methyl groups.